

# Emergence and coherence of oscillations in star networks of stochastic excitable elements

Justus A. Kromer,<sup>1,\*</sup> Lutz Schimansky-Geier,<sup>1,2,†</sup> and Alexander B. Neiman<sup>3,‡</sup>

<sup>1</sup>*Department of Physics, Humboldt-Universität zu Berlin,  
Newtonstr. 15, 12489 Berlin, Germany*

<sup>2</sup>*Bernstein Center for Computational Neuroscience Berlin, Germany*

<sup>3</sup>*Department of Physics and Astronomy and Neuroscience Program,  
Ohio University, Athens, Ohio 45701, USA*

## Abstract

We study the emergence and coherence of stochastic oscillations in star networks of excitable elements in which peripheral nodes receive independent random inputs. A biophysical model of a distal branch of sensory neuron in which peripheral nodes of Ranvier are coupled to a central node by myelinated cable segments is used along with a generic model of networked stochastic active rotators. We show that coherent oscillations can emerge due to stochastic synchronization of peripheral nodes and that the degree of coherence can be maximized by tuning the coupling strength and the size of the network. Analytical results are obtained for the strong coupling regime of the active rotator network. In particular, we show that in the strong coupling regime the network dynamics can be described by an effective single active rotator with rescaled parameters and noise.

PACS numbers: 87.19.ll, 87.19.lb, 87.19.lc, 05.45.Xt, 05.10.Gg

---

\* justuskr@physik.hu-berlin.de

† alsg@physik.hu-berlin.de

‡ neimana@ohio.edu

## I. INTRODUCTION

Spontaneous oscillations are common in biological systems on diverse levels ranging from subcellular and single cell [1, 2] up to cell networks, e.g. in the central nervous system [3, 4]. In many instances, these oscillations are noisy and can be modeled by single or coupled stochastic excitable elements [5] forming complex networks [6–8]. The coherence of noise-induced oscillations can be maximized by tuning the noise intensity (coherence resonance) [9], the coupling strength (array-enhanced coherence resonance) [10, 11], and by varying the number of coupled excitable elements (system size coherence resonance) [12, 13] or the network topology [14].

A structure, whereby few nodes, or hubs, are linked to many other nodes, is a typical motif in topologies of scale-free random and regular networks. A star-type topology, such as shown in Fig. 1, underlines a common situation when peripheral nodes  $P_n$ ,  $P_m$ , are not coupled directly, but through a central hub,  $C$ . Several studies addressed peculiar dynamics of star networks of *deterministic* oscillators [15–18], including the phenomenon of remote synchronization [19, 20].

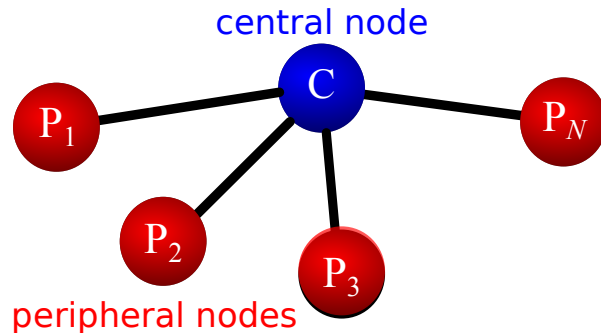


FIG. 1. Color online. Star network considered throughout the paper. Peripheral excitable elements  $P_n$  are linked to the central excitable hub  $C$ . For the model of a distal ending of the branched myelinated axon, peripheral and central elements refer to the nodes of Ranvier, linked by myelinated segments.

This paper is focused on star networks of stochastic excitable elements. One particular example, which motivated this study, comes from the morphology and dynamics of primary sensory neurons, which possess branched myelinated structures in their peripheral terminals [21–24]. Axons of such a neuron can be viewed as a tree-like cable those myelinated seg-

ments link active excitable elements, known as nodes of Ranvier [25]. Myelin terminates at the peripheral nodes, which receive sensory inputs via unmyelinated thin processes. In such a structure, action potentials or spikes can be initiated in several zones due to stochastic and independent inputs to peripheral nodes, resulting in highly non-linear interactions [26]. Notable examples are the muscle spindle sensory neurons, which possess multiple spike initiation zones [25] and show noisy periodic discharges [27]. Drawing in Fig. 1 then represents a distal branch of a myelinated axon where peripheral nodes  $P_k$  receive independent stochastic inputs and are linked by myelinated segments to the central node C, connected to the rest of the axon. We study the emergence of spontaneous oscillations and determinants of oscillation coherence in such a structure. Two types of models for active nodes are used for the excitable elements of the star network. A Hodgkin-Huxley model, which we study by the use of numerical simulations, and an active rotator for which we perform analytical calculations.

The paper is organized as follows. Models and numerical methods, as well as a brief summary of the related single node dynamics, are presented in Sec. II. Stochastic dynamics of the star network of excitable nodes of Ranvier, modeled by a Hodgkin-Huxley type system, is studied numerically in Sec. III A. Then, the star network of stochastic active rotators is analyzed in Sec. III B.

## II. MODELS AND METHODS

In the present paper, we are interested in the stochastic dynamics of excitable elements linked in a star motif such as the one shown in Fig. 1. Peripheral nodes ( $P_k$ ) receive independent stochastic inputs and are coupled to the central hub (C). Random inputs to peripheral nodes may elicit a large event or spike, which in turn may fire up the central node. In the following, we denote the time of the  $j$ th spike of the central node by  $t_j^C$  and that of the  $j$ th spike of the  $n$ th peripheral node by  $t_j^{P_n}$ . The sequences of spike times form corresponding spike trains. Our primary interest is the statistics of a spike train generated at the central node.

### A. Spike train statistics

The coherence of spiking is characterized using the statistics of interspike intervals (ISIs)  $\Delta t_j^k := t_{j+1}^k - t_j^k$ , where the subscripts  $k = C, P_n$  indicate the node, e.g. central or peripheral, and  $j = 1, \dots, J$ , with  $J$  being the number of spikes generated by the  $k$ -th node. The mean firing rate  $r^k$  of a node is defined as reciprocal of the mean ISI and the coefficient of variation (CV)  $C_V^k$  is defined as the ratio of ISI standard deviation and the mean ISI, i.e.

$$r^k = \langle \Delta t_j^k \rangle^{-1}, \quad C_V^k = r^k \sqrt{\langle (\Delta t_j^k - \langle \Delta t_j^k \rangle)^2 \rangle}. \quad (1)$$

Averages were taken over the sequence of ISIs obtained from the spike trains of the central and the individual peripheral nodes, respectively.

### B. Hodgkin-Huxley type model

We use a discrete model [28, 29] for an axon branch consisting of a central node of Ranvier connected to  $N$  peripheral nodes by myelinated segments. The total current of the  $k$ -th peripheral node is given by

$$\pi \mu d \left( C_n \dot{V}_k + I_{\text{ion}} \right) = i_{\text{ext}} + \frac{V_0 - V_k}{R},$$

where  $\mu$  and  $d$  are the length and diameter of the node, respectively;  $C_n$  is the node's capacitance per unit area;  $I_{\text{ion}}$  is the ionic current density;  $i_{\text{ext}}$  the external current, i.e. sensory input to a peripheral node, and  $R$  is the resistance of the myelinated segment. Similarly, for the central node,

$$\pi \mu d \left( C_n \dot{V}_0 + I_{\text{ion}} \right) = \frac{1}{R} \sum_{k=1}^N (V_k - V_0).$$

For a myelinated cable segment of the diameter  $d$  and the length  $L_m$ , the resistance can be calculated as  $R = 4L_m\rho/(\pi d^2)$ , where  $\rho = 200 \, \Omega \text{ cm}$  is the axoplasmic resistivity. Dividing  $R$  by the surface area of the node and taking its reciprocal provides the coupling coefficient in units of Siemens per area:  $\kappa = d/(4\mu L_m\rho)$ . Although we will use  $\kappa$  as the control parameter, it is useful to provide its value for a  $5 \, \mu\text{m}$ -diameter axon with  $\mu = 1 \, \mu\text{m}$  long nodes of Ranvier, connected by  $L_m = 500 \, \mu\text{m}$  long myelinated segment:  $\kappa = 125 \text{ mS/cm}^2$ .

In the following we consider a model for the node of Ranvier, which contains only sodium and leak ionic currents. For simplicity we consider identical nodes and so the ionic current

is  $I_{\text{ion}} = I_{\text{Na}} + I_{\text{L}}$ . For the sodium current we use the Hodgkin-Huxley (HH) type kinetics [30],  $I_{\text{Na}} = g_{\text{Na}} m^3 h$ , where  $m, h$  are activation and inactivation variables, and  $g_{\text{Na}}$  is the maximum value of the Na conductance. The model's equations are:

$$\begin{aligned} C_n \dot{V}_0 &= -g_{\text{Na}} m_0^3 h_0 (V_0 - V_{\text{Na}}) - g_{\text{L}} (V_0 - V_{\text{L}}) + \kappa \sum_{k=1}^N (V_k - V_0), \\ C_n \dot{V}_k &= -g_{\text{Na}} m_k^3 h_k (V_k - V_{\text{Na}}) - g_{\text{L}} (V_k - V_{\text{L}}) + \kappa (V_0 - V_k) + I_{\text{ext}} + \sqrt{2D} \xi_k(t), \\ \dot{m}_{0,k} &= \alpha_m(V_{0,k})(1 - m_{0,k}) - \beta_m(V_{0,k})m_{0,k}, \\ \dot{h}_{0,k} &= \alpha_h(V_{0,k})(1 - h_{0,k}) - \beta_h(V_{0,k})h_{0,k}. \end{aligned} \quad (2)$$

In Eq. (2) the gating kinetics of all nodes is assumed to be identical with rate functions [30],

$$\begin{aligned} \alpha_m(V) &= 1.314(V + 20.4)/\{1 - \exp[-(V + 20.4)/10.3]\}, \\ \beta_m(V) &= -0.0608(V + 25.7)/\{1 - \exp[(V + 25.7)/9.16]\}, \\ \alpha_h(V) &= -0.068(V + 114)/\{1 - \exp[(V + 114)/11]\}, \\ \beta_h(V) &= 2.52/\{1 + \exp[-(V + 31.8)/13.4]\}. \end{aligned} \quad (3)$$

The external current applied to the peripheral nodes has a constant component  $I_{\text{ext}}$  and independent white noise  $\xi_k(t)$  with the intensity  $D$  and

$$\langle \xi_k(t) \rangle = 0 \text{ and } \langle \xi_k(t) \xi_j(t') \rangle = \delta(t - t') \delta_{kj}. \quad (4)$$

Angular brackets  $\langle . \rangle$  stand for the ensemble average. Electrical parameters of the model are as follows  $C_n = 2 \mu\text{F}/\text{cm}^2$ ,  $V_{\text{L}} = 80 \text{ mV}$ ,  $V_{\text{Na}} = 50 \text{ mV}$ ,  $g_{\text{Na}} = 1100 \text{ mS}/\text{cm}^2$ ,  $g_{\text{L}} = 20 \text{ mS}/\text{cm}^2$ . The coupling  $\kappa$  and the constant external current  $I_{\text{ext}}$  are the control parameters.

The coupled stochastic differential equations (2) were integrated using the Euler-Maruyama method with a time step of  $10^{-4} \text{ ms}$ . A spike time for a node is recorded when the voltage crossed a threshold of  $20 \text{ mV}$  with a positive slope. Sequences of the spike times of the  $k$ -th node  $\{t_j^k\}$  were recorded during  $T = 1.2 \times 10^6 \text{ ms}$  (1200s) long simulations.

### C. Active rotator model

Active rotator models subject to noise are commonly used in studies of collective dynamics in large networks of excitable elements [31–35] or mixtures of excitable and oscillatory elements [36]. The state of an active rotator is given by its phase  $\psi$ . Phase, time, and all parameters are dimensionless values. The phase dynamics can be described as an overdamped

motion in the tilted periodic potential,

$$U(\psi) = -\omega\psi + V(\psi), \quad (5)$$

where  $\omega$  represents the tilt, which can be considered as an input to the rotator, and  $V(\psi)$  is  $2\pi$  periodic. There exists a critical tilt  $\omega_c$  at which the extrema of  $U(\psi)$  vanish, corresponding to a saddle-node bifurcation. The rotator is excitable for  $\omega < \omega_c$ , that is, an additional input, e.g. noise, is required for the rotator to overcome the potential barrier and generate an event. The oscillatory regime occurs when  $\omega > \omega_c$ .

In the present paper, we consider two particular choices for  $V(\psi)$ : the cosine potential  $V_{\cos}(\psi)$  and a potential  $V_{\text{opt}}(\psi)$  introduced in Ref. [37], which provides more coherent sequences of events,

$$V_{\cos}(\psi) = -\cos \psi, \quad V_{\text{opt}}(\psi) = \frac{\Delta}{\epsilon} \exp[\epsilon(1 - \cos \psi)]. \quad (6)$$

The potential  $V_{\text{opt}}$  approaches the cosine potential for  $\epsilon \rightarrow 0$ , whereas large values of  $\epsilon \gg 1$  yield a delta-like potential barrier. The parameter  $\Delta$  scales the barrier height and is set to

$$\Delta = \left[ \exp \left( \epsilon - \frac{1}{2} + \sqrt{\epsilon^2 + \frac{1}{4}} \right) \sqrt{1 - \frac{1}{\epsilon^2} \left( \frac{1}{2} - \sqrt{\epsilon^2 + \frac{1}{4}} \right)^2} \right]^{-1}, \quad (7)$$

which rescales the maximum value of  $V'_{\text{opt}}(x)$  to one. With this normalization both  $V_{\cos}$  and  $V_{\text{opt}}$  potentials yield the transition from the excitable to oscillatory regime at the critical tilt  $\omega_c = 1$ .

The active rotators are coupled by a sine function of the phase differences, which is often used in networks of active rotators [31, 33, 35, 36]. We distinguish between the central node with phase  $\theta$  and a set of  $N$  peripheral nodes with phases  $\phi_n$ ,  $n = 1, \dots, N$ . The equations for the central ( $\theta$ ) and peripheral ( $\phi_n$ ) nodes are,

$$\begin{aligned} \dot{\theta} &= \omega_{\theta} + G(\theta) + \kappa \sum_{n=1}^N \sin(\phi_n - \theta) + \sqrt{2D_{\theta}} \xi_{\theta}(t), \\ \dot{\phi}_n &= \omega_{\phi_n} + G(\phi_n) + \kappa \sin(\theta - \phi_n) + \sqrt{2D_{\phi_n}} \xi_{\phi_n}(t), \end{aligned} \quad (8)$$

where  $G(x) = -V'_{\cos}(x)$  or  $G(x) = -V'_{\text{opt}}(x)$ . The  $\theta$ -node is parametrized by  $0 < \omega_{\theta} < 1$  and the coupling strength  $\kappa$ . The  $n$ -th peripheral node is parametrized by the driving parameters  $\omega_{\phi_n}$  and the coupling strength  $\kappa$ . Furthermore, peripheral nodes are excited by independent

Gaussian white noises with intensities  $D_{\phi_n}$ . The Gaussian noises  $\xi_k(t)$  are defined as in Eq. (4) where  $j, k = \phi_n, \theta$ . We also introduce noise to the central node, but in order to model the situation in the branched myelinated axon, we will assume that its intensity is much smaller than those of the driver noises in peripheral nodes,  $D_\theta \ll D_{\phi_n}$ . Nevertheless, our analytical results are valid for arbitrary choices of the noise intensities.

An active rotator generates an event or spike when its state variable ( $\phi_n$  or  $\theta$ ) crosses  $2\pi$  with a positive slope. We perform a phase reset after each  $2\pi$ -crossing by setting the respective phase to zero. Numerically, the reset is realized by subtracting  $2\pi$  from  $\phi$  whenever  $\phi$  is larger than  $2\pi$ . This prevents the generation of spikes due to a crossing of  $2\pi$  with negative phase velocity. Note that this setup allows for phases in the range  $(-\infty, 2\pi)$ .

Numerical integration of Eqs. (8) was performed using the Euler-Maruyama method. The integration time step was set to the minimum value of  $10^{-3}/(D_{\phi_n}\kappa)$  and  $5 \times 10^{-3}$ . Simulations were stopped after  $10^6$  spikes of the central and peripheral nodes were detected or a maximum simulation time of  $10^8$  was reached.

Statistics of spiking events generated by a single stochastic rotator,

$$\dot{\psi} = \omega - V'(\psi) + \sqrt{2D}\xi(t). \quad (9)$$

can be calculated analytically. In particular, an ISI corresponds to the first passage of  $2\pi$  when  $\psi$  has initially started at zero. For the one-dimensional Brownian motion described by Eq. (9) an iterative scheme has been developed in Refs. [38, 39] and, in case of a tilted periodic potential, simplified formulas for the mean first passage time (corresponding to the mean ISI) and the variance of the first passage time distribution (corresponding to the variance of ISIs) have been developed in Refs. [37, 40]. Applying these results to Eq. (9) with a spike generated at  $\psi = 2\pi$  and an instantaneous phase reset to  $\psi = 0$ , the mean ISI is given by

$$\langle \Delta t \rangle = \frac{\int_0^{2\pi} dx \int_{x-2\pi}^x dy \frac{\Phi(x)}{\Phi(y)}}{D \left(1 - e^{-\frac{2\pi\omega}{D}}\right)}, \quad (10)$$

and the variance of ISIs by

$$\text{var}(\Delta t) = \frac{2 \int_0^{2\pi} dx \left( \int_{x-2\pi}^x dy \Phi(y)^{-1} \right)^2 \int_x^{x+2\pi} dz \Phi(z)\Phi(x)}{D^2 \left(1 - e^{-\frac{2\pi\omega}{D}}\right)^3}, \quad (11)$$

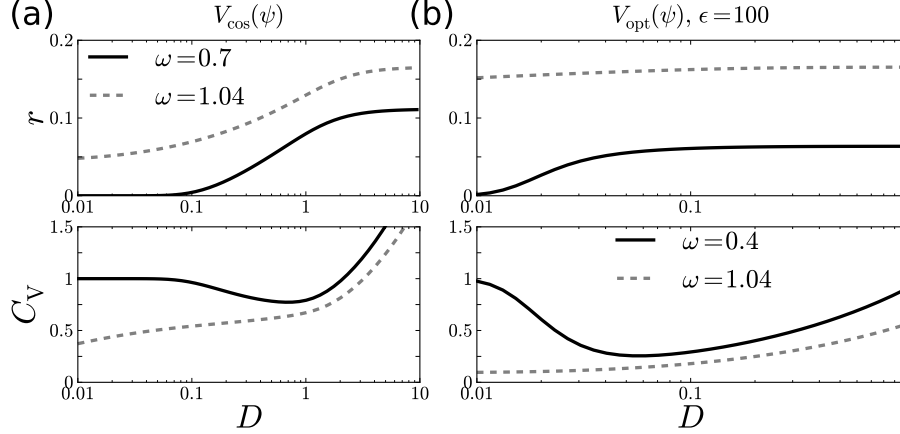


FIG. 2. Dependence of the mean firing rate  $r$  (top) and  $C_V$  (bottom) on noise intensity  $D$  for different values of  $\omega$ , of a single active rotator, Eq. (9), for the two potentials, Eq. (6), (a) and (b) with indicated value of  $\epsilon$ , respectively.

where  $\Phi(x) = \exp[U(x)/D]$ . We use these formulas to calculate the firing rate  $r = 1/\langle\Delta t\rangle$  and the CV  $C_V = \sqrt{\text{var}(\Delta t)}/\langle\Delta t\rangle$ , which is in agreement with Eq. (1). Figure 2 shows the mean firing rate and the CV for  $\omega < \omega_c$ , i.e. in the excitable regime, and for one  $\omega > \omega_c$ , i.e. in the oscillatory regime, respectively for both potentials used in this study as functions of the noise intensity. In the excitable regime, the CV passes through a minimum for both potentials, demonstrating the phenomenon of coherence resonance [9]. As expected, noise-induced oscillations are more coherent for the potential  $V_{\text{opt}}$ . In the oscillatory regime, noise merely degrades the oscillation coherence, as CV increases monotonically with  $D$ .

### III. RESULTS

#### A. Noise-induced spiking in a star network with Hodgkin-Huxley nodes

We start with the deterministic dynamics ( $D = 0$ ) of a single uncoupled peripheral node, i.e.  $N = 1$ ,  $\kappa = 0$  in Eqs. (2). For  $I_{\text{ext}} < 29.06 \mu\text{A}/\text{cm}^2$ , the node is at the stable resting equilibrium. This equilibrium undergoes a subcritical Andronov-Hopf bifurcation at  $I_{\text{ext}} \approx 29.06 \mu\text{A}/\text{cm}^2$ . Oscillations on the large-amplitude limit cycle cause a periodic sequence of full-size action potentials for  $I_{\text{ext}} > 29.06 \mu\text{A}/\text{cm}^2$ .

With the addition of stochastic input the single node exhibits the phenomenon of coherence resonance [9] in the excitable regime,  $I_{\text{ext}} < 29.06 \mu\text{A}/\text{cm}^2$ , demonstrated in Fig. 3. For



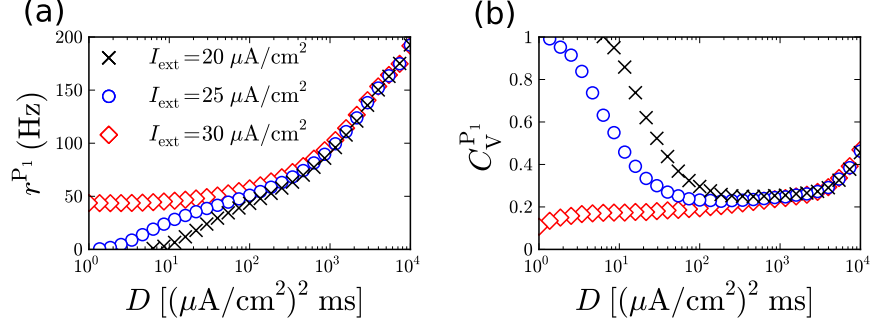


FIG. 3. Color online. Dependence of the mean firing rate  $r^{P_1}$  and  $C_V^{P_1}$  on noise intensity  $D$  of a single uncoupled peripheral HH-type node for the indicated values of  $I_{\text{ext}}$ .

$I_{\text{ext}} < 29.06 \mu\text{A}/\text{cm}^2$  and weak noise, the node generates action potentials extremely rarely, resulting in a low firing rate and a large CV (black and blue symbols in Fig. 3a,b). With the increase of the noise intensity, the firing rate increases and the ISI sequence becomes progressively more regular, as indicated by the decrease of the CV. Strong noise eventually results in an increase of the CV. In contrast, in the regime of periodic spiking,  $I_{\text{ext}} > 29.06 \mu\text{A}/\text{cm}^2$ , the CV increases monotonically with  $D$ , (red squares in Fig. 3b), as noise merely worsens the coherence of periodic spiking.

When  $N$  excitable nodes are coupled in the star network, stochastic dynamics of the central node depends crucially on the coupling strength. For extremely weak coupling, peripheral nodes fire asynchronously. This results in sparse and irregular firing of the central node, see Fig. 4a1. Weak coupling synchronizes the network leading to coherent spiking, see Fig. 4a2. Finally, strong coupling makes the system stiff, so that inputs to peripheral nodes may not be enough to sustain coherent periodic firing. Consequently, nodes fire in synchrony, but less coherently, as Fig. 4a3 indicates. This dynamics is summarized in Fig. 5a. The main feature is the existence of an optimal value of the coupling strength, which maximizes the firing rate of peripheral and the central nodes and minimizes the variability of their firing.

Another feature is concerned with the scaling with the number of peripheral nodes  $N$  for the case of strong coupling, which is illustrated in Fig. 6a. The strong coupling regime is of particular interest as it represents the situation for primary endings of muscle spindles sensory neurons. For example, the length of myelinated segments in peripheral branches of cat muscle spindles ranges over  $58 - 192 \mu\text{m}$  [41], which for a cable diameter of  $1 - 6 \mu\text{m}$  corresponds to the coupling strength  $\kappa = 65 - 1300 \text{ mS}/\text{cm}^2$ , causes strong coupling between

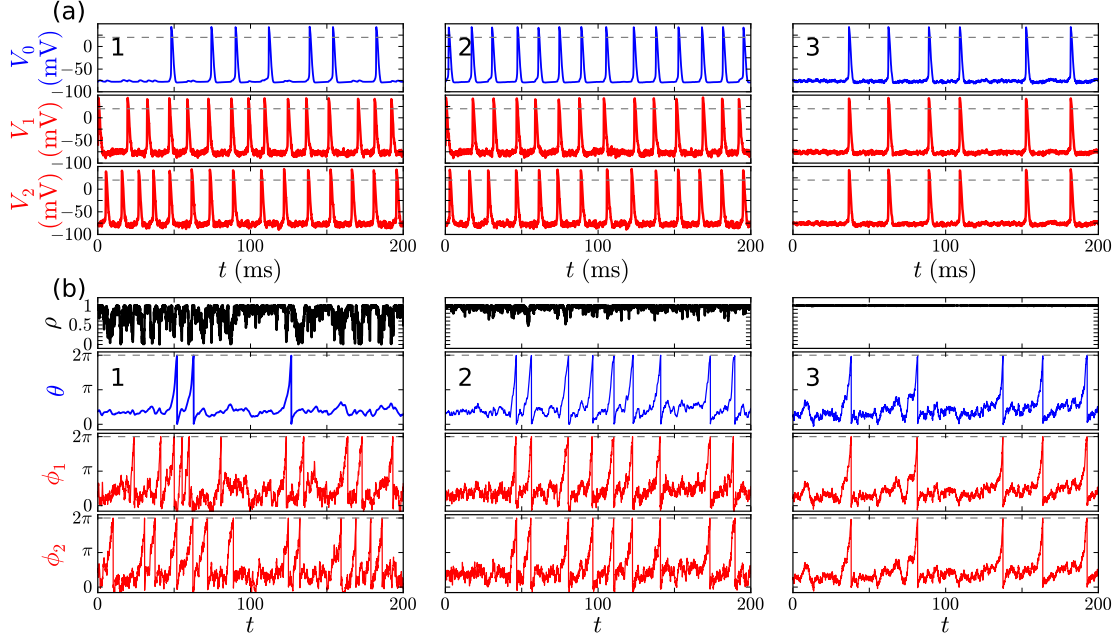


FIG. 4. Color online. State traces of a star network of HH (a) and active rotator (b) stochastic excitable elements for different values of the coupling strengths,  $\kappa$ . The central node is plotted blue and peripherals red, respectively. Spiking thresholds are indicated by the dashed horizontal lines. (a): Voltage traces of a star network with HH nodes, Eqs. (2) with  $N = 2$  peripheral nodes. The parameters are:  $\kappa = 0.3$  (1),  $\kappa = 0.625$  (2),  $\kappa = 100 \text{ mS/cm}^2$  (3), respectively;  $I_{\text{ext}} = 20 \text{ } \mu\text{A/cm}^2$ ,  $D = 500 (\text{ } \mu\text{A/cm}^2)^2\text{ms}$ . (b): Traces of the phases in a similar network of active rotators, Eq. (8), with  $G(x) = -V'_{\text{cos}}(x)$ . The trace of the Kuramoto order parameter, Eq. (12), is illustrated by the black line. The parameters are:  $\kappa = 0.328$  (1),  $\kappa = 2.147$  (2),  $\kappa = 57.646$  (3), respectively;  $D_\theta = 0$ ,  $D_{\phi_n} = D_{\phi_m} = 0.4$ ,  $\omega_\theta = \omega_{\phi_n} = \omega_{\phi_m} = 0.9$ . The average degrees of synchronization  $\bar{\rho}$ , Eq. (18), are 0.78 (1), 0.95 (2), and 1.0 (3), respectively.

central and peripheral nodes.

In a small star network,  $N < 3$ , the variability of the spiking of the central node is suppressed by the increase of the number peripheral nodes as indicated by smaller values of  $C_V$  in Fig. 6a (bottom). On the contrary, the operation mode of the peripheral nodes is critical for the scaling for larger  $N$  and strong coupling. If peripheral nodes are excitable, the dependencies of  $r^C$  and  $C_V^P$  on  $N$  are non-monotonic. In that case, we find an optimal network size for which the firing rate attains a maximum and the spiking is most coherent. Thus, in the biologically-plausible strong coupling regime, the network demonstrates system

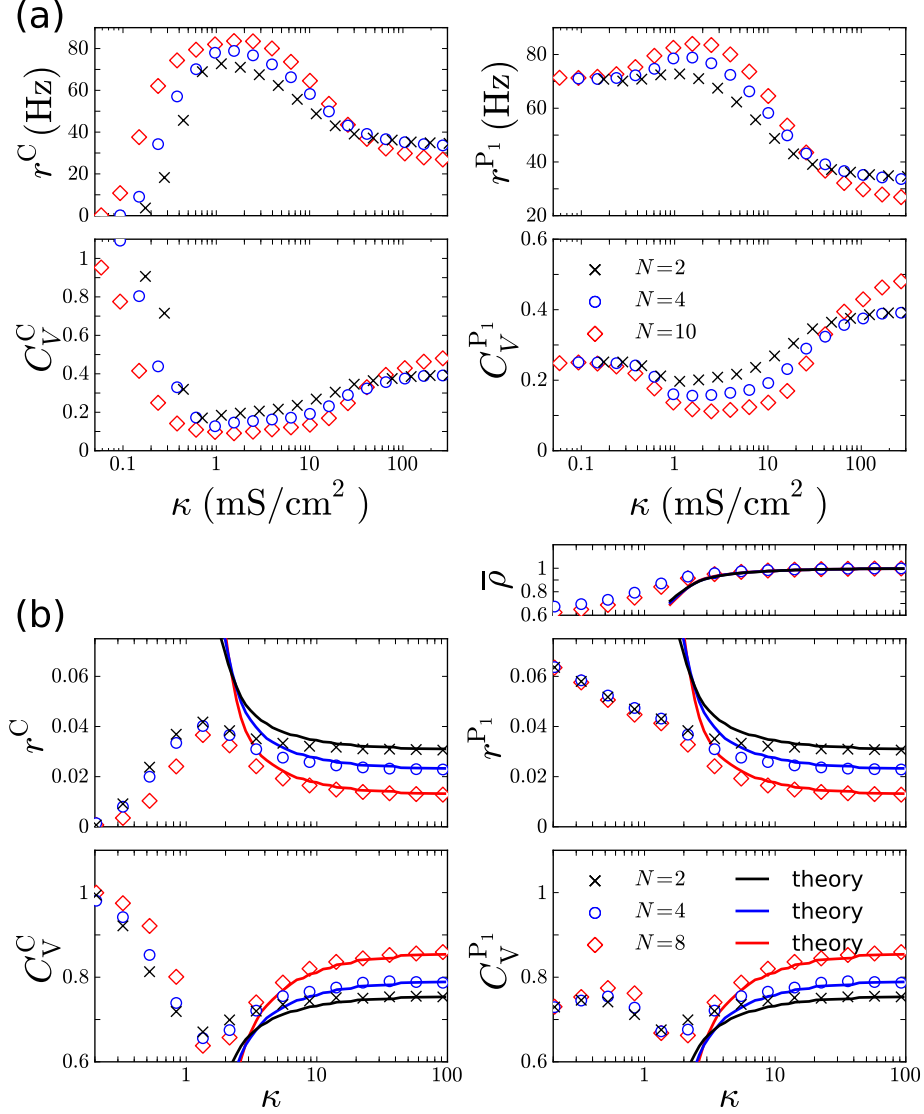


FIG. 5. Color online. Effect of coupling on the firing statistics of star networks with HH (a) and active rotator (b) nodes. Firing rates  $r$  and CVs  $C_V$  versus the coupling strength  $\kappa$  for the indicated numbers of peripheral nodes  $N$ . Left columns correspond to the central node and right columns to the first peripheral node, respectively. (a): Star network of HH-type nodes. The parameters are:  $I_{\text{ext}} = 20 \mu\text{A}/\text{cm}^2$  and  $D = 500 (\mu\text{A}/\text{cm}^2)^2\text{ms}$ . (b): Star network of active rotators, Eq. (8), with cosine potential,  $G(x) = -V'_{\text{cos}}(x)$ . The upper right panel shows the time-averaged order parameter  $\bar{\rho}$ . Symbols correspond to numerical simulation, solid lines show analytical approximation. The parameters are:  $\omega_{\phi_n} = \omega_{\phi_m} = \omega_{\theta} = 0.9$ ,  $D_{\theta} = 0$ , and  $D_{\phi_n} = D_{\phi_m} = 0.4$ .

size resonance [12, 13]. In contrast, if peripherals operate in the oscillatory regime, the firing

rate increases, while the variability decreases monotonically.

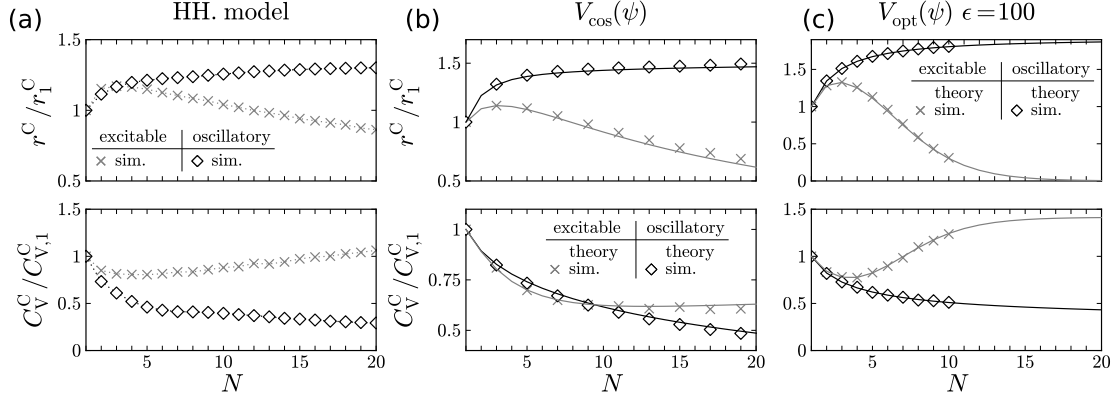


FIG. 6. System size effect on the firing statistics of star networks of HH-type (a) and active rotator nodes (b,c) in the strong coupling regime. Upper panels show the firing rate of the central node and lower panels show the CV versus the number of peripheral nodes. Two regimes of peripheral nodes, excitable and oscillatory, are shown. Firing rates and CVs are normalized by their values at  $N = 1$ ,  $r_1^C$  and  $C_{V,1}^C$ , respectively, in order to show the relative change of these measures. (a): Star network of HH-type nodes. Symbols show results of numerical simulations. The parameters are:  $I_{\text{ext}} = 1 \mu\text{A}/\text{cm}^2$  (excitable regime) and  $I_{\text{ext}} = 60 \mu\text{A}/\text{cm}^2$  (oscillatory regime),  $D = 500 (\mu\text{A}/\text{cm}^2)^2\text{ms}$ . (b): Star network of active rotators with cosine potential,  $V_{\cos}$ . The parameters are:  $\omega_\theta = 0.3$ ,  $D_\theta = 0$ ,  $\kappa = 100$ ;  $\omega_{\phi_n} = \omega_{\phi_m} = 0.7$ ,  $D_{\phi_n} = D_{\phi_m} = 10$  (excitable regime) and  $\omega_{\phi_n} = \omega_{\phi_m} = 1.5$ ,  $D_{\phi_n} = D_{\phi_m} = 5$  (oscillatory regime). (c): Star network of active rotators with potential  $V_{\text{opt}}$ . The parameters are:  $\omega_\theta = 0$ ,  $D_\theta = 0$ ,  $\kappa = 1000$ ,  $D_{\phi_n} = D_{\phi_m} = 0.3$ ;  $\omega_{\phi_n} = \omega_{\phi_m} = 0.1$  (excitable regime) and  $\omega_{\phi_n} = \omega_{\phi_m} = 1.1$  (oscillatory regime). On panels b,c symbols correspond to numerical simulations and lines show theory.

## B. Star network of active rotators

In this section we show that in the strong coupling limit the star network of stochastic active rotators can be replaced with a single effective rotator with an effective drive and noise. However, first we illustrate that the dynamics of the star network of active rotators is qualitatively akin to that of networked HH nodes. Figure 4b shows the effect of regularization of the nodes' firing for an optimal coupling strength. This can be also seen in Fig. 5b, which shows the firing rate and CV versus  $\kappa$  for the central node and peripherals. Similar to the

star network of HH nodes, the firing rate passes through a maximum and the CV through a minimum when peripherals are in excitable regime. Furthermore, in case of strong coupling, the network shows the effect of system size resonance for both potentials used, as shown in Fig. 6b,c.

Next, we study the spiking in the strong coupling regime, corresponding to a model of a branched myelinated axon. In that case, as illustrated in Fig. 4, the membrane potentials in the HH network as well as the phases in the active rotator network, are synchronized. In order to quantify the degree of synchronization of the peripheral nodes, we use the time-dependent Kuramoto order parameter:

$$\rho(t) e^{I\Psi(t)} := \frac{1}{N} \sum_{i=1}^N e^{I\phi_i}. \quad (12)$$

Its absolute value  $\rho(t)$ , yields the degree of synchronization of all peripheral nodes, i.e.  $\rho(t) = 1$  corresponds to perfect synchronization of the peripherals, while  $\rho(t) = 0$  indicates the completely asynchronous regime.  $\Psi(t)$  is the peripherals' mean field phase. Using the definition of the order parameter, Eq. (12), and the  $\theta$ -dynamics, Eq. (8), we obtain for the central node,

$$\dot{\theta} = \omega_\theta + G(\theta) + N\rho\kappa \sin(\Psi - \theta) + \sqrt{2D_\theta}\xi_\theta(t). \quad (13)$$

Thus, the central node is only coupled to the phase of the mean field of the peripherals  $\Psi$  with the rescaled coupling strength  $N\rho(t)\kappa$ . Consequently, the central node is most affected if the peripheral nodes are synchronized.

The magnitude and the phase of the order parameter can be obtained by following an approach of Ref. [34]. Taking the time derivative of the order parameter, Eq. (12),

$$\frac{d}{dt} (\rho e^{I\Psi}) = \dot{\rho} e^{I\Psi} + I\dot{\Psi} \rho e^{I\Psi} = \frac{I}{N} \sum_{i=1}^N \dot{\phi}_i e^{I\phi_i},$$

and dividing both sides by  $e^{I\Psi}$ , we obtain for the imaginary part

$$\rho\dot{\Psi} = \frac{1}{N} \sum_{i=1}^N \dot{\phi}_i \cos(\phi_i - \Psi). \quad (14)$$

Here, the phase difference  $\delta_i^\Psi := \phi_i - \Psi$  between the  $i$ -th peripheral node and the mean field appears, which we split into two parts. First, the phase difference between the mean field and the phase of the central node  $\delta^{\theta,\Psi} := \theta - \Psi$  and, second, the differences between the

phase of the central node and those of the  $N$  peripheral nodes  $\delta_i^\theta := \theta - \phi_i$ . It holds that  $\delta_i^\Psi = -\delta_i^\theta + \delta^{\theta, \Psi}$ . For strong coupling,  $N\rho\kappa \gg \max(1, \omega_\theta, D_\theta)$  and  $\kappa \gg \max(1, \omega_{\phi_n}, D_{\phi_n})$ , both phase differences,  $\delta^{\theta, \Psi}$  and  $\delta_i^\theta$  become small parameters and so the cosine in Eq. (14) can be linearized, yielding

$$\rho\dot{\Psi} = \frac{1}{N} \sum_{i=1}^N \dot{\phi}_i + \mathcal{O}((\delta_i^\Psi)^2). \quad (15)$$

Using Eq. (8), and the definition of the Kuramoto order parameter, Eq. (12), we obtain in the first order in  $\delta_i^\Psi$

$$\rho\dot{\Psi} = \langle \omega_\phi \rangle_N + \langle G(\phi_i) \rangle_N + \kappa\rho \sin(\theta - \Psi) + \sqrt{\frac{2\langle D_\phi \rangle_N}{N}} \xi_\Psi(t), \quad (16)$$

where  $\langle \cdot \rangle_N$  denotes averages over all peripheral nodes, i.e.  $\langle D_\phi \rangle_N := \frac{1}{N} \sum_{n=1}^N D_{\phi_n}$  and  $\langle \omega_\phi \rangle_N := \frac{1}{N} \sum_{n=1}^N \omega_{\phi_n}$ . In Eq. (16),  $\xi_\Psi(t)$  is a white Gaussian noise, which has an intensity that is inversely proportional to the network size and proportional to the average noise intensity of the peripheral nodes [34].

If  $G(x) = -V'_{\cos}(x)$ , the average of  $G(x)$  can be simplified using the definition of the Kuramoto order parameter, Eq. (12), yielding similar results as in [34],

$$\rho\dot{\Psi} = \langle \omega_\phi \rangle_N - \rho \sin(\Psi) + \kappa\rho \sin(\theta - \Psi) + \sqrt{\frac{2\langle D_\phi \rangle_N}{N}} \xi_\Psi(t). \quad (17)$$

Small deviations from the perfectly-synchronized state can be accounted for by representing  $\rho$  by its long-time average,

$$\bar{\rho} := \frac{1}{T} \int_0^T dt' \rho(t), \quad (18)$$

where  $T \gg 1/r^i$ ,  $r^i$  are the mean firing rates of peripheral and central nodes, with  $i = C, P_1, P_2, \dots, P_N$ . This results in the strong coupling approximation for the mean field phase,

$$\dot{\Psi} = \frac{\langle \omega_\phi \rangle_N}{\bar{\rho}} - \sin(\Psi) + \kappa \sin(\theta - \Psi) + \sqrt{\frac{2\langle D_\phi \rangle_N}{\bar{\rho}^2 N}} \xi_\Psi(t). \quad (19)$$

For an arbitrary potential, an equation of similar form can be obtained by considering only the zeroth order contributions of  $\delta_i^\Psi$  in Eq. (16), i.e.  $\phi_i = \Psi$  and  $\rho = 1$ . This yields

$$\dot{\Psi} = \langle \omega_\phi \rangle_N + G(\Psi) + \kappa \sin(\theta - \Psi) + \sqrt{\frac{2\langle D_\phi \rangle_N}{N}} \xi_\Psi(t), \quad \rho = 1. \quad (20)$$

In either case, the dynamics of the strongly-coupled star network is described by two coupled rotators in which the central node, Eq. (13), is coupled to a second rotator, which represents the dynamics of the mean field phase of the peripheral nodes. In the case of cosine potential this two-rotator representation reads,

$$\begin{aligned}\dot{\theta} &= \omega_{\theta} - \sin(\theta) + N\bar{\rho}\kappa \sin(\Psi - \theta) + \sqrt{2D_{\theta}}\xi_{\theta}(t), \\ \dot{\Psi} &= \frac{\langle\omega_{\phi}\rangle_N}{\bar{\rho}} - \sin(\Psi) + \kappa \sin(\theta - \Psi) + \sqrt{\frac{2\langle D_{\phi}\rangle_N}{\bar{\rho}^2 N}}\xi_{\Psi}(t).\end{aligned}\tag{21}$$

In order to obtain analytical results for the ISI statistics of the central node, we consider the dynamics of the phase difference  $\delta^{\theta,\Psi}(t) = \theta(t) - \Psi(t)$ , which is small in the strong coupling regime,  $\delta^{\theta,\Psi}(t) \ll 1$ . Hence, linearizing the coupling functions in Eq. (21) yields,

$$\begin{aligned}\dot{\theta} &= \omega_{\theta} - \sin(\theta) - N\bar{\rho}\kappa \delta^{\theta,\Psi} + \sqrt{2D_{\theta}}\xi_{\theta}(t), \\ \dot{\Psi} &= \frac{\langle\omega_{\phi}\rangle_N}{\bar{\rho}} - \sin(\Psi) + \kappa \delta^{\theta,\Psi} + \sqrt{\frac{2\langle D_{\phi}\rangle_N}{\bar{\rho}^2 N}}\xi_{\Psi}(t).\end{aligned}\tag{22}$$

Furthermore, as we show in Appendix A, the phase difference  $\delta^{\theta,\Psi}(t)$  can be approximated by

$$\delta^{\theta,\Psi}(t) \approx \frac{\omega_1}{\kappa_1} + \frac{\sqrt{2D_1}}{\kappa_1} \xi_1(t),\tag{23}$$

where  $\omega_1 = \omega_{\theta} - \langle\omega_{\phi}\rangle_N/\bar{\rho}$ ,  $\kappa_1 = \kappa(N\bar{\rho} + 1)$ , and  $\xi_1(t)$  is a Gaussian noise, given by

$$\sqrt{2D_1}\xi_1(t) = \sqrt{2D_{\theta}}\xi_{\theta}(t) - \sqrt{\frac{2\langle D_{\phi}\rangle_N}{\bar{\rho}^2 N}}\xi_{\Psi}(t),\tag{24}$$

with  $D_1 = D_{\theta} + \langle D_{\phi}\rangle_N/(N\bar{\rho}^2)$ . Putting the approximation for  $\delta^{\theta,\Psi}(t)$  into Eq. (22) with (24), we obtain an effective single-rotator approximation for the star network with rescaled driving parameter and noise intensity,

$$\dot{\theta} = \omega_{\text{mod}}(\bar{\rho}, N) - \sin(\theta) + \sqrt{2D_{\text{mod}}(\bar{\rho}, N)}\xi(t).\tag{25}$$

The first term on the r.h.s. stands for the effective drive

$$\omega_{\text{mod}}(\bar{\rho}, N) = \frac{\langle\omega_{\phi}\rangle_N}{\bar{\rho}} + \frac{1}{1 + N\bar{\rho}} \left( \omega_{\theta} - \frac{\langle\omega_{\phi}\rangle_N}{\bar{\rho}} \right).\tag{26}$$

The effective noise intensity  $D_{\text{mod}}(\bar{\rho}, N)$  accounts for the impact of white Gaussian noises of all nodes in the network and is given by

$$D_{\text{mod}}(\bar{\rho}, N) = \frac{D_{\theta} + N\langle D_{\phi}\rangle_N}{(1 + N\bar{\rho})^2}.\tag{27}$$

Note that the dependence on the coupling strength  $\kappa$  is captured by the average degree of synchronization  $\bar{\rho}$ . The latter can be calculated numerically using the self-consistent approach presented in Appendix B. In the general case of arbitrary functions  $G(x)$ , one obtains a similar approximation in the limit of perfectly-synchronized peripherals,  $\bar{\rho} = 1$ , which reads

$$\dot{\theta} = \omega_{\text{mod}}(1, N) + G(\theta) + \sqrt{2D_{\text{mod}}(1, N)}\xi(t). \quad (28)$$

Note that this result does not account for the influence of the coupling strength and solely holds in the limit  $\kappa \rightarrow \infty$ . We remark that the effective dynamics of the mean field phase of the peripheral nodes  $\Psi$ , is described by an identical equation.

The mean firing rate and the CV of the central node can then be calculated from the equations for the mean ISI and the ISI variance of a single active rotator, Eqs. (10) and (11), respectively, with modified driving parameter, Eq. (26), and noise intensity Eq. (27). Consequently, the ISI statistics of the central hub of the star network is that of a single active rotator, Eq. (9), with  $\omega = \omega_{\text{mod}}(\bar{\rho}, N)$  and  $D = D_{\text{mod}}(\bar{\rho}, N)$ . The statistics for the latter is illustrated in the respective plots in Fig. 2 and summarized in Fig. 7 as contour plots. These theoretical results are compared to simulations in Fig. 5b, showing very good correspondence for strong coupling. In particular, the theory correctly accounts for the decrease of the firing rate and the increase of the CV in the range of strong coupling, which is also observed in the star network of HH-type nodes.

Since lower values of the coupling strength enter only through a slightly smaller average degree of synchronization in Eq. (25), the shaping of the dependence of the firing rate and the CV on  $N$  is caused by slightly asynchronous behavior of the peripheral nodes. For a fixed number of peripheral nodes this slight asynchrony causes larger tilt  $\omega_{\text{mod}}(\bar{\rho}, N)$  of the corresponding potential and stronger noise  $D_{\text{mod}}(\bar{\rho}, N)$ . As can be seen in the contour plots in Fig. 7, this always causes an increase of the firing rate. However, the CV is reduced only if  $\omega_{\text{mod}}(\bar{\rho}, N) < 1$  and  $D_{\text{mod}}(\bar{\rho}, N)$  is sufficiently small, i.e. when the single active rotator given by Eq. (25) is excitable and below the coherence resonance minimum of the CV.

In the limit of perfectly synchronous spiking of all peripherals, i.e.  $\bar{\rho} = 1$ , the strong coupling approximation, Eq. (28), holds for arbitrary function  $G(x)$  and the effective parameters  $\omega_{\text{mod}}$  and  $D_{\text{mod}}$  depend only on the network size  $N$  and the nodes' parameters. The related strong coupling approximations for the ISI statistics of the central node for two



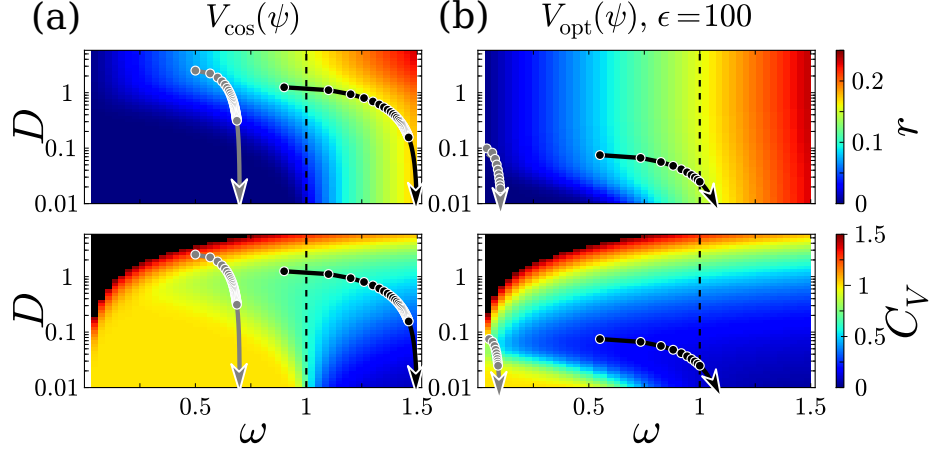


FIG. 7. Color online. Dependence of the mean firing rate  $r$  and  $C_V$  on noise intensity  $D$  and input  $\omega$  of a single active rotator for the two potentials  $V_{\cos}$  (a) and  $V_{\text{opt}}$  (b). Dashed black lines indicate the transition from excitable to oscillatory regime. Black color on lower panels marks a region with CVs above 1.5. Curves and circles on panels a and b show parametric plots of  $(\omega, D) = (\omega_{\text{mod}}(1, N), D_{\text{mod}}(1, N))$ , for the effective noise intensity and the driving parameter of the networked elements obtained from Eqs. (26) and (27). They correspond to the curves depicted in Figs. 6b and 6c, respectively. Arrows indicate the direction of increasing network size  $N$ . Gray lines and circles refer to curves for excitable and black lines and circles to those for oscillatory peripherals depicted in Fig. 6b,c.

choices of the potential with  $G(x) = -V'_{\cos}(x)$  and  $G(x) = -V'_{\text{opt}}(x)$ , corresponding simulation results, and simulation results for the HH-type nodes are compared in Fig. 6. As can be seen from the figure, all three models possess qualitatively similar dependencies of the firing rate and the CV vs  $N$ . In the strong coupling regime theory fits perfectly the results from simulations.

The dependencies  $\omega_{\text{mod}}(1, N)$  and  $D_{\text{mod}}(1, N)$  can be mapped onto contour maps of the firing rate and the CV of the single rotator as parametric curves, shown in Fig. 7. Indeed, the influence of the number of peripherals  $N$  on the ISI statistics can be easily understood by considering the corresponding dependence of the effective parameters  $\omega_{\text{mod}}$  and  $D_{\text{mod}}$  on  $N$ . For  $N = 1$ , we find  $\omega_{\text{mod}}(1, 1) = (\omega_{\theta} + \langle \omega_{\phi} \rangle_N)/2$  and  $D_{\text{mod}}(1, 1) = (D_{\theta} + \langle D_{\phi} \rangle_N)/4$ . In contrast, in the limit of large  $N$ , we obtain  $\omega_{\text{mod}}(1, \infty) = \langle \omega_{\phi} \rangle_N$  and  $D_{\text{mod}}(1, \infty) = 0$ . Thus, the behavior for large  $N$  is determined by the peripheral nodes. Furthermore, an optimal network size, with respect to a minimal CV, can be observed whenever the trace of

$(\omega_{\text{mod}}(1, N), D_{\text{mod}}(1, N))$  crosses the region of low CVs in Fig. 7. This corresponds to the case when the peripherals are excitable and strong noise is present in the system, i.e. when  $D_\theta + \langle D_\phi \rangle_N$  is large.

#### IV. CONCLUSION

We showed that coherent oscillations can emerge in a star network in which peripheral excitable elements receive random and independent inputs and are coupled via a central excitable hub. The coherence of synchronous stochastic spiking can be maximized by changing the coupling strength between peripheral and central nodes and by the network size, which indicates that the observed phenomenon is a specific type of system size [12, 34, 42] and array-enhanced coherence resonance [10, 11].

We developed an analytical approximation for a generic model of a star network of active rotators. The theory shows that in the strong coupling regime the peripheral nodes can be replaced by an effective rotator describing their mean field phase. Using this approach we were able to predict the ISI statistics of synchronized oscillations and the optimal network size with respect to a maximal firing rate and a minimal ISI variability. This is a specific type of system size resonance [12, 34, 42], observed in all-to-all coupled noisy elements, whereby addition of elements into the network reduces the effective noise in the system. In case of the star network, variation of the network size modifies the excitability of the system, in addition to the noise reduction mentioned above. A reduction of the coupling strength leads to an increase of the firing rate and, in certain parameter ranges, to a reduction of ISI variability. The latter leads to array-enhanced coherence resonance, i.e. maximal coherence at a finite coupling strength [10, 11]. According to our analytical results, this is caused by a slight desynchronization of the oscillations of the peripheral nodes. A similar effect has been observed in large networks of globally coupled active rotators [34, 43].

The emergence of coherent oscillations was investigated using a HH-type node dynamics in which the transition to oscillatory behavior occurs via subcritical Andronov-Hopf bifurcation and in active rotator models in which the transition occurs via a saddle-node bifurcation. This indicates that the observed phenomenon is independent of the respective type of bifurcation and is a generic phenomenon in star networks of excitable elements, similar to emergence of pacemakers in excitable media [44]. Our results suggest a biologically

plausible mechanism for the emergence of noisy periodic discharges observed in branched myelinated axons of some sensory neurons, such as muscle spindles [27]. In particular, in sensory neurons of cat muscle spindles the length of primary myelinated segments ranges from 58 to 192  $\mu\text{m}$  and the distance from the first branching point to 1–9 peripheral nodes ranges over 250 – 560  $\mu\text{m}$  [41]. With such relatively short myelinated segments, electrotonically coupled nodes are likely to operate in the strong coupling regime studied here.

## V. ACKNOWLEDGEMENTS

The authors thank D.F. Russell and J.T.C. Schwabedal for valuable discussions. JK and LSG have been funded by IRTG 1740/TRP 2011/50151-0, DFG / FAPESP and by the BMBF (FKZ: 01GQ1001A). AN gratefully acknowledges the support of NVIDIA Corp. with the donation of the Tesla K40 GPU used for this research.

### Appendix A: Linear approximation for the phase difference, $\delta^{\theta,\Psi}$

The dynamics of  $\delta^{\theta,\Psi}(t)$  is found by subtracting the individual phase dynamics in Eq. (21). It gives

$$\dot{\delta}^{\theta,\Psi} = \omega_1 - \sin\left(\frac{\beta^{\theta,\Psi} + \delta^{\theta,\Psi}}{2}\right) + \sin\left(\frac{\beta^{\theta,\Psi} - \delta^{\theta,\Psi}}{2}\right) - \kappa_1 \delta^{\theta,\Psi} + \sqrt{2D_1} \xi_1(t), \quad (\text{A1})$$

with  $\beta^{\theta,\Psi} = \theta + \Psi$ , the difference of the input parameters  $\omega_1 = \omega_\theta - \frac{\langle \omega_\phi \rangle_N}{\bar{\rho}}$ , and the effective coupling strength  $\kappa_1 = \kappa(N\bar{\rho} + 1)$ . The difference of the two noises yields a new Gaussian white noise  $\xi_1(t)$ , with intensity  $D_1 = D_\theta + \langle D_\phi \rangle_N / N\bar{\rho}^2$ . Linearization with respect to  $\delta^{\theta,\Psi}$  yields

$$\dot{\delta}^{\theta,\Psi} = \omega_1 - \left( \cos\left(\frac{\beta^{\theta,\Psi}}{2}\right) + \kappa_1 \right) \delta^{\theta,\Psi} + \sqrt{2D_1} \xi_1(t). \quad (\text{A2})$$

Furthermore, we can neglect the cosine term inside the brackets since it is bounded by one and therefore small compared to  $\kappa_1$ . This yields

$$\dot{\delta}^{\theta,\Psi} = \omega_1 - \kappa_1 \delta^{\theta,\Psi} + \sqrt{2D_1} \xi_1(t). \quad (\text{A3})$$

Thus,  $\delta^{\theta,\Psi}(t)$  is an Ornstein-Uhlenbeck process, which is Gaussian and can be characterized by a time-dependent mean and variance. In the strong coupling regime,  $\kappa_1$  is large and the mean and variance approach their stationary limits fast. Then, it is sufficient to approximate  $\delta^{\theta,\Psi}(t)$  as the constant mean value  $\omega_1/\kappa_1$  plus a white Gaussian noise given by Eq.(23).

## Appendix B: Self-consistent calculation of $\bar{\rho}$

In order to find an approximation for  $\bar{\rho}$  in Eq. (25), we evaluate the time average of the degree of synchronization  $\rho$ , Eq. (18). Using the definition of the Kuramoto order parameter Eq. (12) and dividing both sides by  $\exp(I\Psi)$ , we find

$$\bar{\rho} = \frac{1}{N} \overline{\sum_{i=1}^N e^{I(\phi_i - \Psi)}} = \frac{1}{N} \overline{\sum_{i=1}^N \cos(\phi_i - \Psi)}. \quad (\text{B1})$$

This follows from the fact that  $\rho$  is real and the mean field phase  $\Psi$  is defined in a way that the imaginary part of the sum vanishes. Next, we introduce the small parameter  $\delta^{\theta, \Psi} = \theta - \Psi$ . Using a corresponding Taylor expansion and the Kuramoto order parameter Eq. (12) for the first order term yields

$$\bar{\rho} \approx \frac{1}{N} \overline{\sum_{i=1}^N \cos(\phi_i - \theta) + \mathcal{O}((\delta^{\theta, \Psi})^2)}. \quad (\text{B2})$$

By introducing the conditioned stationary probability distribution  $p(\theta|\bar{\rho})$  of  $\theta$  for given  $\bar{\rho}$ . and that of the phases  $\phi_i$  of the  $i$  peripheral node for a given particular value of  $\theta$ ,  $p_i(\phi_i|\theta)$ , we can apply a similar approach as Tessone et. al. [34] and rewrite Eq. (B2) in case of strong coupling into the self-consistent equation:

$$\bar{\rho} = \frac{1}{N} \int_0^{2\pi} d\theta \, p(\theta|\bar{\rho}) \sum_{i=1}^N \int_0^{2\pi} d\phi_i \, \cos(\phi_i - \theta) p_i(\phi_i|\theta). \quad (\text{B3})$$

Next, we apply standard methods for stochastic systems [45], and consider the *Fokker-Planck equation* for  $p_i(\phi_i|\theta)$  following from the  $\phi_i$ -dynamics, Eq. (8) for a constant  $\theta$  first. We are interested in the stationary probability distribution and have to take into account the instantaneously phase reset  $\phi_i = 2\pi \rightarrow \phi_i = 0$ . Such a problem corresponds to the exit problem of a Brownian particle, which starts at  $\phi_i = 0$  and leaves the region  $(-\infty, 2\pi)$  through the point  $\phi_i = 2\pi$  for the first time. The *Fokker-Planck equation* for the stationary probability distribution of this problem reads

$$0 = \partial_t p_i(\phi_i|\theta) = \partial_{\phi_i} (\partial_{\phi_i} F_i(\phi_i, \theta) + D_{\phi_i} \partial_{\phi_i}) p_i(\phi_i|\theta) + r^{\phi_i}(\theta) \delta(\phi_i). \quad (\text{B4})$$

$\delta(\phi_i)$  is the Dirac delta function and  $r^{\phi_i}(\theta)$  is the amount of probability that is reset per unit time and, thus, corresponds to the stationary firing rate of the system for a given  $\theta$ . The

drift term is the deterministic flow with  $F_i(\phi_i, \theta) = U(\phi_i) - \kappa_\phi \cos(\theta - \phi_i)$  and  $U$  defined in Eq. (5). Note that driving  $\omega_{\phi_i}$  and noise intensity  $D_{\phi_i}$  of the individual peripherals differ. Equation (B4) is complemented by an absorbing boundary  $p_i(2\pi|\theta) = 0$  at the upper end of the region and the probability vanishes as  $\phi_i \rightarrow -\infty$ . By integrating Eq. (B4) one immediately gets

$$p_i(\phi_i|\theta)\partial_{\phi_i}F_i(\phi_i, \theta) + D_{\phi_i}\partial_{\phi_i}p_i(\phi_i|\theta) = -r^{\phi_i}(\theta) H(\phi_i). \quad (\text{B5})$$

$H(x)$  is the Heaviside step function, which results from the integration of the delta function in Eq. (B4) and accounts for the nonzero probability flux between reset and threshold. Using variations of constants, this can be integrated and, considering the boundary conditions, we obtain

$$p_i(\phi_i|\theta) = \frac{r^{\phi_i}(\theta)}{D_{\phi_i}} \exp\left(-\frac{F_i(\phi_i, \theta)}{D_{\phi_i}}\right) \int_{\phi_i}^{2\pi} d\phi' \exp\left(\frac{F_i(\phi', \theta)}{D_{\phi_i}}\right) H(\phi'). \quad (\text{B6})$$

Afterwards, the firing rate  $r^{\phi_i}(\theta)$  can be obtained from the normalization condition resulting in an expression for the firing rate:

$$r^{\phi_i}(\theta) = D_{\phi_i} \left( \int_{-\infty}^{2\pi} d\phi \exp\left(-\frac{F_i(\phi, \theta)}{D_{\phi_i}}\right) \int_{\phi}^{2\pi} d\phi' \exp\left(\frac{F_i(\phi', \theta)}{D_{\phi_i}}\right) H(\phi') \right)^{-1}.$$

One can apply a similar approach for  $p(\theta|\bar{\rho})$  for a given, fixed value of  $\bar{\rho}$ . To this end, we approximate the  $\theta$ -dynamics by the single-node description, Eq. (25). The corresponding *Fokker-Planck equation* for the stationary distribution becomes

$$0 = \partial_\theta (\partial_\theta U(\theta, \bar{\rho}) + D_{\text{mod}}(\bar{\rho}, N) \partial_\theta) p(\theta|\bar{\rho}) + r^\theta(\bar{\rho}) \delta(\theta). \quad (\text{B7})$$

$r^\theta(\bar{\rho})$  is the stationary firing rate of the  $\theta$ -rotator for given  $\bar{\rho}$ . The potential  $U(\theta, \bar{\rho})$  depends on the degree of synchronization via the tilt  $\omega_{\text{mod}}(\bar{\rho}, N)$  given in Eq. (26). Additionally, the modified noise intensity  $D_{\text{mod}}(\bar{\rho}, N)$  is given in Eq. (27). Solving Eq. (B7), we obtain

$$p(\theta|\bar{\rho}) = \frac{r^\theta(\bar{\rho})}{D_{\text{mod}}(\bar{\rho}, N)} \exp\left(-\frac{V(\theta, \bar{\rho})}{D_{\text{mod}}(\bar{\rho}, N)}\right) \int_{\theta}^{2\pi} d\theta' \exp\left(\frac{V(\theta', \bar{\rho})}{D_{\text{mod}}(\bar{\rho}, N)}\right) H(\theta'). \quad (\text{B8})$$

Again, the firing rate  $r^\theta(\bar{\rho})$  can be obtained from the normalization condition.

Using the results for  $p(\theta|\bar{\rho})$  and  $p(\phi_i|\theta)$ , we can calculate the right-hand side of the self-consistent Eq. (B3) numerically. For the evaluation, we fix  $\bar{\rho}$  and calculate the corresponding

right-hand side. Continuing this for  $\bar{\rho} \in [0, 1]$ , we search for intersections of the left-hand and right-hand side. For all considered parameter sets, we observed only one intersection. Implementing this into the single-node representation, Eq. (25), yields a full strong coupling approximation of the dynamics, which is used in Fig. 5b.

- 
- [1] K. Kruse and F. Jülicher, *Current Opinion in Cell Biology* **17**, 20 (2005).
  - [2] B. N. Kholodenko, *Nature Reviews Molecular Cell Biology* **7**, 165 (2006).
  - [3] G. Buzsáki, *Rhythms of the Brain* (Oxford University Press, New York, 2006).
  - [4] O. Sporns, *Networks of the Brain* (MIT Press, Cambridge MA, 2011).
  - [5] B. Lindner, J. García-Ojalvo, A. Neiman, and L. Schimansky-Geier, *Physics Reports* **392**, 321 (2004).
  - [6] M. E. Newman, *SIAM Review* **45**, 167 (2003).
  - [7] S. Boccaletti, V. Latora, Y. Moreno, M. Chavez, and D.-U. Hwang, *Physics Reports* **424**, 175 (2006).
  - [8] A. Arenas, A. Díaz-Guilera, J. Kurths, Y. Moreno, and C. Zhou, *Physics Reports* **469**, 93 (2008).
  - [9] A. S. Pikovsky and J. Kurths, *Physical Review Letters* **78**, 775 (1997).
  - [10] A. Neiman, L. Schimansky-Geier, A. Cornell-Bell, and F. Moss, *Physical Review Letters* **83**, 4896 (1999).
  - [11] C. Zhou, J. Kurths, and B. Hu, *Physical Review Letters* **87**, 098101 (2001).
  - [12] R. Toral, C. Mirasso, and J. Gunton, *EPL (Europhysics Letters)* **61**, 162 (2003).
  - [13] A. Pikovsky and A. Zaikin, *AIP Conference Proceedings* **665**, 561 (2003).
  - [14] M. Gosak, D. Korošak, and M. Marhl, *Physical Review E* **81**, 056104 (2010).
  - [15] H. Kitajima and J. Kurths, *Physica A* **388**, 4499 (2009).
  - [16] H. Kitajima and T. Yoshihara, *Physica D* **241**, 1804 (2012).
  - [17] O. Burylko, Y. Kazanovich, and R. Borisjuk, *Physica D* **241**, 1072 (2012).
  - [18] Y. Kazanovich, O. Burylko, and R. Borisjuk, *Physica D* **261**, 114 (2013).
  - [19] M. Frasca, A. Bergner, J. Kurths, and L. Fortuna, *International Journal of Bifurcation and Chaos* **22**, 1250173 (2012).
  - [20] A. Bergner, M. Frasca, G. Sciuto, A. Buscarino, E. J. Ngamga, L. Fortuna, and J. Kurths,

- Physical Review E **85**, 026208 (2012).
- [21] A. Iggo and A. R. Muir, The Journal of Physiology **200**, 763 (1969).
  - [22] J. A. Pruszyński and R. S. Johansson, Nature Neuroscience (2014).
  - [23] L.-Y. Lee and J. Yu, Comprehensive Physiology (2014).
  - [24] G. S. Bewick and R. W. Banks, Pflügers Archiv-European Journal of Physiology **467**, 175 (2015).
  - [25] D. Quick, W. Kennedy, and R. Poppele, Neuroscience **5**, 109 (1980).
  - [26] J. P. Eagles and R. L. Purple, Brain research **77**, 187 (1974).
  - [27] R. Banks, M. Hulliger, K. Scheepstra, and E. Otten, The Journal of Physiology **498**, 177 (1997).
  - [28] J. P. Keener and J. Sneyd, *Mathematical Physiology*, 2nd ed., Interdisciplinary Applied Mathematics, Vol. 8/1 (Springer, New York, 2009).
  - [29] B. Ermentrout and D. H. Terman, *Foundations of Mathematical Neuroscience*, Interdisciplinary Applied Mathematics, Vol. 35 (Springer, New York, 2010).
  - [30] C. C. McIntyre, A. G. Richardson, and W. M. Grill, Journal of Neurophysiology **87**, 995 (2002).
  - [31] S. Shinomoto and Y. Kuramoto, Progress of Theoretical Physics **75**, 1105 (1986).
  - [32] C. Kurrer and K. Schulten, Physical Review E **51**, 6213 (1995).
  - [33] M. A. Zaks, A. B. Neiman, S. Feistel, and L. Schimansky-Geier, Physical Review E **68**, 066206 (2003).
  - [34] C. J. Tessone, A. Scirè, R. Toral, and P. Colet, Physical Review E **75**, 016203 (2007).
  - [35] B. Sonnenschein, M. A. Zaks, A. B. Neiman, and L. Schimansky-Geier, The European Physical Journal Special Topics **222**, 2517 (2013).
  - [36] B. Sonnenschein, T. K. D. Peron, F. A. Rodrigues, J. Kurths, and L. Schimansky-Geier, The European Physical Journal B **87**, 1 (2014).
  - [37] B. Lindner, M. Kostur, and L. Schimansky-Geier, Fluctuation and Noise Letters **1**, R25 (2001).
  - [38] L. Pontryagin, A. Andronov, and A. Witt, Zhurnal Eksperimental'noi i Teoreticheskoi Fiziki **3**, 165 (1933), reprinted in *Noise in nonlinear dynamical systems*, 1989, ed. by F. Moss and P. V. E. McClintock (Cambridge University Press, Cambridge), vol. 1, pp. 329-348.
  - [39] A. J. F. Siegert, Physical Review **81**, 617 (1951).

- [40] P. Reimann, C. Van den Broeck, H. Linke, P. Hänggi, J. M. Rubi, and A. Pérez-Madrid, Physical Review E **65**, 031104 (2002).
- [41] R. W. Banks, D. Barker, and M. Stacey, Philosophical Transactions of the Royal Society B: Biological Sciences **299**, 329 (1982).
- [42] A. Pikovsky, A. Zaikin, and M. A. de la Casa, Physical Review Letters **88**, 050601 (2002).
- [43] T. Kanamaru and M. Sekine, IEICE TRANSACTIONS on Fundamentals of Electronics, Communications and Computer Sciences **86**, 2197 (2003).
- [44] P. Jung and P. Gailey, Annalen der Physik **9**, 697 (2000).
- [45] C. W. Gardiner, *Handbook of Stochastic Methods*, 2nd ed., edited by H. Haken, Springer Series in Synergetics (Springer, Berlin, 1985).